Dynamic Behavior of Intermediate Adsorbates to Control Activity and Product Selectivity in Heterogeneous Catalysis: Methanol Decomposition on $Pt/TiO_2(110)$

Can Liu,[a] Bang Lu,[b] Hiroko Ariga-Miwa,[c] Shohei Ogura,[d] Takahiro Ozawa,[e] Katsuyuki Fukutani,[e] Min Gao,[f] Jun-ya Hasegawa,[a] Ken-ichi Shimizu,[a] Kiyotaka Asakura,[a] and Satoru Takakusagi*[a]

[a] Institute for Catalysis, Hokkaido University, Sapporo, Hokkaido 001-0021, Japan

[b] Division of Quantum Science and Engineering, Graduate School of Engineering, Hokkaido University, Sapporo, Hokkaido 001-0021, Japan

[c] Innovation Research Center for Fuel Cells and Hydrogen, The University of Electro-Communications, 1-5-1 Chofugaoka, Chofu, Tokyo 182-8585, Japan

[d] School of Engineering, Tokyo Denki University, 5 Senju Asahi-cho, Adachi-ku, Tokyo 120-8 551, Japan

[e] Institute of Industrial Science, The University of Tokyo, 4-6-1 Komaba, Meguro-ku, Tokyo 153-8505, Japan

[f] Institute for Chemical Reaction Design and Discovery (ICReDD), Hokkaido University, Sapporo, Hokkaido 001-0021, Japan

KEYWORDS: methanol decomposition • $Pt/TiO_2(110)$ • surface diffusion • spillover • reverse spillover • scanning tunneling microscopy (STM) • density functional theory (DFT) calculation • temperature-programmed desorption (TPD)

ABSTRACT: Dynamic behavior of intermediate adsorbates, such as diffusion, spillover, and reverse spillover, has a strong influence on the catalytic performance in oxide-supported metal catalysts. However, it is challenging to elucidate how the intermediate adsorbates move on the catalyst surface and find active sites to give the corresponding products. In this study, the effect of the dynamic behavior of methoxy intermediate on methanol decomposition on a $Pt/TiO_2(110)$ surface has been clarified by combination of scanning tunneling microscopy (STM), temperature-programmed desorption (TPD), and density functional theory (DFT) calculations. The methoxy intermediates were formed by the dissociative adsorption of methanol molecules on Pt nanoparticles at room temperature, followed by spillover to the $TiO_2(110)$ support surface. TPD results showed that the methoxy intermediates were thermally decomposed at >350 K on the Pt sites to produce CO (dehydrogenation) and CH_4 (C-O bond scission). A decrease of the Pt nanoparticle density lowered the activity for the decomposition reaction and increased the selectivity toward CH_4, which indicates that the reaction is controlled by diffusion and reverse spillover of the methoxy intermediates. Time-lapse STM imaging and DFT calculations revealed that the methoxy intermediates migrate on the five-fold coordinated Ti (Ti_{5c}) sites along the [001] or [1$\bar{1}$0] direction with the aid of hydrogen adatoms bonded to the bridging oxygens (O_{br}) and can move over the entire surface to seek and find active Pt sites. This work offers an in-depth understanding of the important role of intermediate adsorbate migration in the control of the catalytic performance in oxide-supported metal catalysts.

Introduction

Heterogeneous catalysts are key materials for the development of a sustainable society and play a critical role in the industrial production of various chemicals.[1,2] The majority of these materials consist of active transition-metal species, typically nanoparticles, which are highly dispersed on powdery oxide supports with large surface areas. The origins of catalytic activity and product selectivity in such oxide-supported metal catalysts are generally explained by different types of active sites, such as metal nanoparticle sites, metal-oxide interfacial sites, and oxide surface sites, where intermediate adsorbates react to give the corresponding products. It should also be noted that the dynamic behavior of the intermediate adsorbates, such as diffusion, spillover, and reverse spillover, has a strong effect on the overall reactivity and reaction kinetics of the oxide-supported metal catalysts.[3-5] For example, methanol adsorbs onto the γ-Al_2O_3 support of Ni/γ-Al_2O_3 catalysts, and is dehydrogenated to produce CO and H_2 by diffusion and reverse spillover to the Ni particle surface.[6] The presence of Ni significantly increases the decomposition rate of methanol, and also changes the product selectivity. Another example is that CO spills over from the Pt nanoparticles onto the TiO_2 support and is oxidized to CO_2 by the removal of an oxygen atom from the TiO_2 lattice.[7]

Atomic-level understanding of the dynamic behavior of intermediate adsorbates and its effect on the catalytic properties of oxide-supported metal catalysts is thus crucial. However, direct observation of such dynamic behavior is still difficult due to the limitations of the characterization techniques available. Scanning tunneling microscopy (STM) is one of the most powerful techniques because it can image individual atoms or molecules on a solid surface and monitor their motion in the presence of reactant gases.[8-11] We have previously reported the first direct visualization of spillover adsorbates emitted from metal nanoparticles onto an oxide support surface by *in situ* time-resolved STM observation.[12] The methanol adsorption behavior on Pt nanoparticles deposited on a TiO_2(110) surface was examined, and the methanol molecules were found to be dissociated on the Pt nanoparticles to produce methoxy intermediates at room temperature, which then spilled over to the five-fold coordinated Ti^{4+} sites (Ti_{5c}) of the TiO_2(110) surface (see Figure 1). The methoxy intermediates were mobile at room temperature and were distributed over the entire TiO_2(110) surface. The following questions must be solved to understand the role of the dynamic behavior of the methoxy intermediates on methanol decomposition reaction on Pt/TiO_2(110). (1) Where do the methoxy intermediates react and decompose at high temperatures? On the Pt sites or TiO_2 sites? (2) How do the methoxy intermediates migrate on the surface to seek and find the active sites? In this study, we examined the thermal decomposition and diffusion of methoxy intermediates on the Pt/TiO_2(110) surface using STM, temperature-programmed desorption (TPD) and density functional theory (DFT) calculations to answer these questions. The results provide new insights into how intermediate adsorbates move on a catalyst surface to reach the active sites in oxide-supported metal catalysts, and show that atomic-level understanding of their dynamic behaviors is crucial to unravel the origins of catalytic activity and product selectivity.

Results and Discussion

Adsorption of Methanol on the Pt/TiO_2(110) surface

Figure 1a shows an STM image of the TiO_2(110) surface after Pt deposition at room temperature, followed by annealing at 473 K for 10 min. The Pt coverage was 0.11 ML, where 1 ML is defined as 5.2×10^{18} /m² based on the TiO_2(1×1) unit cell. The Pt nanoparticles were uniformly distributed on the TiO_2(110) surface with a density of 5.4×10^{16} /m². Histograms of the apparent height and diameter of the Pt nanoparticles are also shown in Figure 1a, where the averages were 0.5±0.2 nm and 2.3±0.6 nm, respectively. It is noted that the height and diameter obtained by STM may not be very accurate because of convolution effects with the STM tip and electronic structure effects. Figure 1b shows an STM image of the Pt/TiO_2(110) surface after exposure to 5 L methanol vapor at room temperature. Additional bright spots were observed on the Ti_{5c} rows, and the coverage was estimated to be 0.14 ML, whereas these were not observed in the absence of Pt nanoparticles. The apparent height was 0.18 nm, and the lateral size was 0.50 nm. We have previously assigned these bright spots to methoxy species

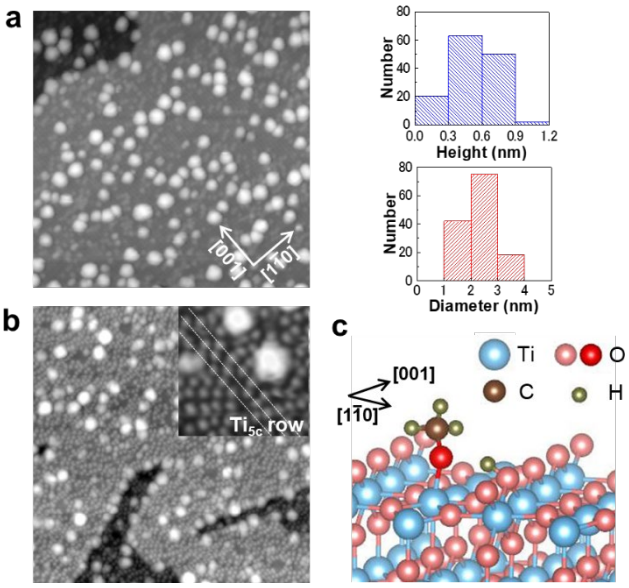

Figure 1. (a) STM image (50×50 nm²) of a Pt/TiO_2(110) surface and histograms of the apparent height and diameter of the Pt nanoparticles. The Pt/TiO_2(110) surface was prepared by Pt deposition (0.11 ML) at room temperature, followed by annealing at 473 K for 10 min. The particle density was 5.4×10^{16} /m². (b) STM image (50×50 nm²) of the Pt/TiO_2(110) surface after exposure to 5 L methanol vapor at room temperature. The inset is magnified image of another area (7.4×7.4 nm²). The methoxy coverage was 0.14 ML. (c) Methoxy intermediate adsorbed on a Ti_{5c} site of a TiO_2(110) surface.

bonded to the Ti_{5c} sites (CH_3O-Ti_{5c} in Figure 1c).[12] The previous *in situ* time-resolved STM studies clearly showed that they were produced by the dissociation of methanol molecules at the periphery of the Pt nanoparticles (Pt-TiO_2 interfacial sites), and then transferred to the Ti_{5c} sites through the spillover process.

Another Pt/TiO_2(110) surface with a smaller Pt loading (0.04 ML) was prepared to observe the dependence of the methanol adsorption property on the Pt nanoparticle density, and the results are shown in Figure 2a. The average height and diameter of the deposited Pt nanoparticles were 0.5±0.2 nm and 2.2±0.4 nm, respectively. The size distribution was similar to that in Figure 1a, which indicates that only the particle density was able to be controlled successfully (2.4×10^{16} /m²). Figure 2b shows an STM image after

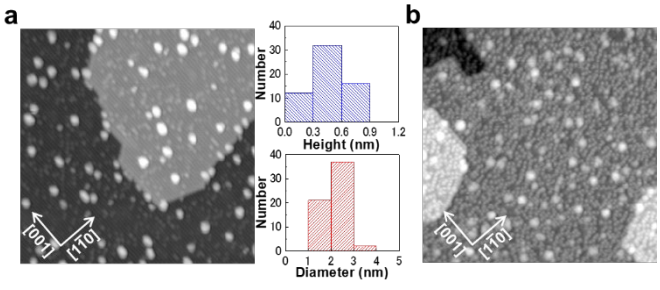

Figure 2. (a) STM image (50×50 nm²) of a Pt/TiO_2(110) surface and histograms of the apparent height and diameter of the Pt nanoparticles. The Pt/TiO_2(110) surface was prepared by Pt deposition (0.04 ML) at room temperature, followed by annealing at 473 K for 10 min. The particle density was 2.4×10^{16} /m². (b) STM image (50×50 nm²) of the Pt/TiO_2(110) surface after exposure to 5 L methanol vapor at room temperature. The methoxy coverage was 0.14 ML.

exposure to 5 L of methanol vapor at room temperature. The methoxy intermediates were observed over the entire surface and the coverage reached 0.14 ML, which is the same as that in Figure 1b. Dependence of methanol exposure on the methoxy coverage was also examined for the two Pt/TiO_2(110) surfaces shown in Figures 1a and 2a (Figure S1). The saturation coverage of the methoxy intermediates was almost identical while the adsorption rate increased with a higher density of Pt nanoparticles. The saturation coverage may be determined by the repulsive interaction between the neighboring methoxy species on the TiO_2(110) surface. It should be noted that methoxy species on bridging oxygen (O_{br}) vacancies which are known to form on a bare TiO_2(110) surface[13, 14](see Figure S2) were rarely observed in Figures 1b and 2b. We have found that density of the O_{br} vacancies in Figures 1a and 2a was less than 0.01 ML, which was negligibly small compared to that on the bare TiO_2(110) surface (~0.06 ML) (Figure S3). This could be attributed to enhanced adsorption of residual water molecules in the UHV chamber due to the presence of Pt nanoparticles, which resulted in filling of the O_{br} vacancies with hydroxyl groups and blocking adsorption of the methoxy species.

We denote the Pt/TiO_2(110) samples with high (Figure 1) and low (Figure 2) densities of Pt nanoparticles as H-Pt/TiO_2(110) and L-Pt/TiO_2(110), respectively.

Effect of methoxy intermediate diffusion on its thermal decomposition on the Pt/TiO_2(110) surface

The thermal decomposition behavior of the methoxy intermediates was investigated for the H-Pt/TO_2(110) and L-Pt/TiO_2(110) samples via TPD measurements. It can be expected that the decomposition behavior of the methoxy intermediates would differ between the two samples if they are decomposed mainly on the Pt sites through diffusion and reverse spillover, whereas they would not differ significantly if most of them are decomposed on the TiO_2 surface.

Figure 3 shows TPD profiles for the methoxy intermediates on the H-Pt/TiO_2(110) and L-Pt/TiO_2(110) surfaces. In the H-Pt/TiO_2(110) sample, the major products were CO (m/z = 28), H_2 (m/z = 2), and CH_4 (m/z = 16), while formaldehyde (H_2CO, m/z = 30) and methanol (CH_2OH, m/z = 31) were also observed as minor products. It is noted that all the products desorbed simultaneously over a wide range of temperatures from ca. 350 K to 650 K. On the other hand, in the L-Pt/TiO_2(110) sample, the desorption peaks were all shifted to higher temperatures, which indicates that the activity for the methoxy decomposition reaction was decreased. The production of CO and H_2 was largely suppressed, and instead CH_4 production was enhanced, i.e., high selectivity toward CH_4. The desorption of the minor products (formaldehyde and methanol) was slightly suppressed in the lower temperature region (<500 K), whereas it did not change much in the higher temperature region (>500 K).

The total amount of desorbed carbonaceous products (CO, CH_4, H_2CO, and CH_3OH) should also be the same for the two samples because the methoxy coverage was the same (0.14 ML). We confirmed that the estimated ratio of the total amount of carbonaceous products for the H- to L-Pt/TiO_2(110) samples was 1.1 based on their TPD peak areas (see Tables S2 and S3). The selectivities toward the carbonaceous products were also estimated to be 31% (CO), 55% (CH_4), 9% (H_2CO), and 5% (CH_3OH) for H-Pt/TiO_2(110), and 12% (CO), 77% (CH_4), 8% (H_2CO), and 3% (CH_3OH) for L-Pt/TiO_2(110), as shown in Tables S2 and S3. Since the TPD results were dependent on the Pt particle density, it can be concluded that most of the methoxy intermediates were decomposed on the Pt sites through diffusion and reverse spillover. Note that since the size distributions and chemical states of the Pt nanoparticles in the H-Pt/TiO_2(110) and L-Pt/TiO_2(110) samples were almost identical even after the samples were heated at 650 K (see STM

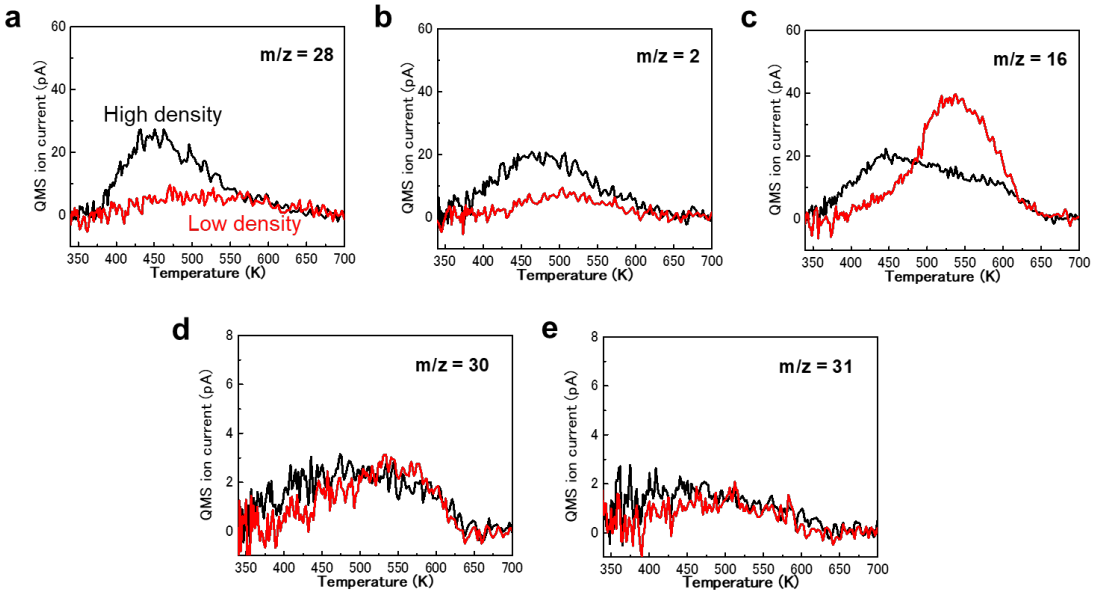

Figure 3. (a) TPD profiles for methoxy intermediates on Pt/TiO_2(110) surfaces with different Pt particle densities. Black curve: high particle density (5.4×10^{16} /m^2, H-Pt/TiO_2(110)), red curve: low particle density (2.4×10^{16} /m^2, L-Pt/TiO_2(110)). (a) CO (m/z = 28), (b) H_2 (m/z = 4), (c) CH_4 (m/z = 16), (d) formaldehyde (m/z = 30), (e) methanol (m/z = 31). Note that the y-axis scale differs between (a)-(c) and (d),(e).

and XPS results in Figures S4 and S5, respectively), the active sites of the two Pt/TiO_2(110) samples were similar during the decomposition reaction. It is worth noticing that the two TPD profiles in Figure 3 were also different from that for the bare TiO_2(110) surface after exposure to 5 L methanol vapor at RT, where only CH_4 was detected as a decomposition product in the temperature range of 550~650 K (Figure S6)[15].

It has been reported that dehydrogenation of methanol to CO and H_2 is the major reaction pathway on flat Pt single-crystal surfaces such as P(111)[16,17] and Pt(100)[18]. A significant difference between such flat surfaces and the Pt nanoparticles is that production of CH_4 from C-O bond scission is observed on the Pt nanoparticles.[15,19,20] For example, when the Pt nanoparticles were supported on an inert Al_2O_3/NiAl(100) surface and heated after exposure to methanol-d_4 (CD_3OD) vapor at low temperature (100 K), CO and D_2 were formed as major products and methane-d_4 (CD_4) as a minor product (<10%).[19] The desorption of CO and CD_4 started at 300~350 K depending on the Pt coverage. These results may indicate that flat terrace sites on the Pt nanoparticles were active for dehydrogenation reaction while specific defect sites such as edge/corner Pt atoms (peripheral Pt atoms in the Pt nanoparticles) were active for CH_4 production.

In the TPD profiles for the methoxy intermediates on the H-Pt/TiO_2(110) surface, the CO/H_2 desorption peaks (black curves in Figures 3a and 3b) were broad and had a tail on the higher temperature side. These results suggest contribution from the methoxy species that diffused over the short to long distance on the TiO_2(110) surface and then reacted on the Pt sites. In contrast, the CH_4 desorption curve (black curve in Figure 3c was more complex. The main feature was similar to the CO/H_2 desorption curves, but an additional peak appeared around 600 K. The main feature was probably due to the methoxy decomposition at the peripheral Pt sites. On the other hand, the temperature range of the additional CH_4 desorption well corresponded to that from methoxy species on the O_{br} vacancies of the TiO_2(110) surface (Figure S6). As illustrated in Figure. S3, most of the oxygen vacancies on the TiO_2(110) surface were converted to the hydroxyl groups after Pt deposition. However, since the hydroxyl groups are desorbed as water at >450 K[21,22], the O_{br} vacancies could be reproduced during the heating in the TPD measurements and work as active sites for the CH_4 formation. It has also been reported that oxygen vacancy formation energy on TiO_2(110) is reduced by Pt deposition[23] and the oxygen vacancies created close to the Pt atoms on TiO_2 work as active sites for efficient C-O bond scission of furfuryl alcohol molecules.[24] Such oxygen vacancies could also be formed on our Pt/TiO_2(110) surfaces and promote the CH_4 production. The higher selectivity to CH_4 in the TPD results for the methoxy intermediates on the L-Pt/TiO2(110) also supports that the Pt-TiO_2 interfacial sites such as peripheral Pt atoms in the Pt nanoparticles and oxygen vacancies close to the Pt nanoparticles efficiently cleaved the C-O bond to produce CH_4 because the diffusing methoxy intermediates firstly reached the Pt-TiO_2 interfacial sites and then other Pt sites. When the particle density was decreased in the L-Pt/TiO_2(110) sample, more time was required for the methoxy intermediates to reach the Pt nanoparticles, and the Pt-TiO_2 interfacial sites were more activated for the arriving methoxy intermediates. Therefore, most of the methoxy intermediates were decomposed at the Pt-TiO_2 interfacial sites to produce CH_4 immediately upon arrival at the Pt nanoparticles and could not reach the other Pt surface sites which are active for CO production. Oxygen vacancies on the TiO_2(110) terraces could also contribute to the CH_4 production as in the case of the H-Pt/TiO_2(110) sample.

Formaldehyde and methanol were also observed as minor products in the TPD results, where their desorption was promoted in the lower temperature region (<500 K) when the density of Pt nanoparticles was increased, which indicates that formaldehyde and methanol would be formed preferentially on the Pt sites by partial dehydrogenation of the methoxy intermediates and by recombination of the methoxy species (CH_3O-Pt) and hydrogen (H-Pt), respectively. On the other hand, in the high temperature region (>500 K), the desorption behaviors were not significantly dependent on the particle density, which may suggest that most of these species were produced on the TiO_2 sites. It has been reported that the methoxy intermediates can be formed on the TiO_2(110) surface in the absence of the Pt nanoparticles by exposure of a clean TiO_2(110) surface to O_2 gas and then to methanol vapor at room temperature, followed by heating at 350 K.[25, 26] The methoxy intermediates are thermally decomposed into formaldehyde and methanol by the disproportionation reaction between two methoxy intermediates and desorb at >550 K.[25] The disproportionation reaction between the two methoxy intermediates might occur to produce formaldehyde and methanol, particularly at >550 K.

Diffusion mechanism of methoxy intermediates on the Pt/TiO_2(110) surface

The TPD results clearly showed that thermal decomposition of the methoxy intermediates on Pt/TiO_2(110) was controlled by their diffusion. However, we have not determined how these intermediates diffuse on the surface and reach the active Pt sites during the decomposition process, and how they become distributed over the entire TiO_2(110) surface after spillover from the Pt nanoparticles in the methanol adsorption process. Sequential STM imaging and DFT calculation were thus performed to elucidate the diffusion mechanism of the methoxy intermediates. Figure 4 shows the results of sequential STM imaging of the methoxy intermediates on the Pt/TiO_2(110) surface. Both the Pt and methoxy intermediate coverages were decreased compared to those shown in Figures 1 and 2 to distinguish and monitor each methoxy species accurately (see the large-scale image (50×50 nm^2) in Figure S7 for reference). Each grid point of the mesh drawn in Figures 4a-4d represents the location of the Ti_{5c} sites, and every methoxy species in the images is annotated by a number. In Figures 4a and 4b, methoxy No. 11 moved to the next Ti_{5c} site along the [001] direction. In Figure 4c, methoxy No. 11 jumped along the [1$\bar{1}$0] direction and landed on the same Ti_{5c} row as methoxy No. 10, followed by the departure of methoxy No. 10 and

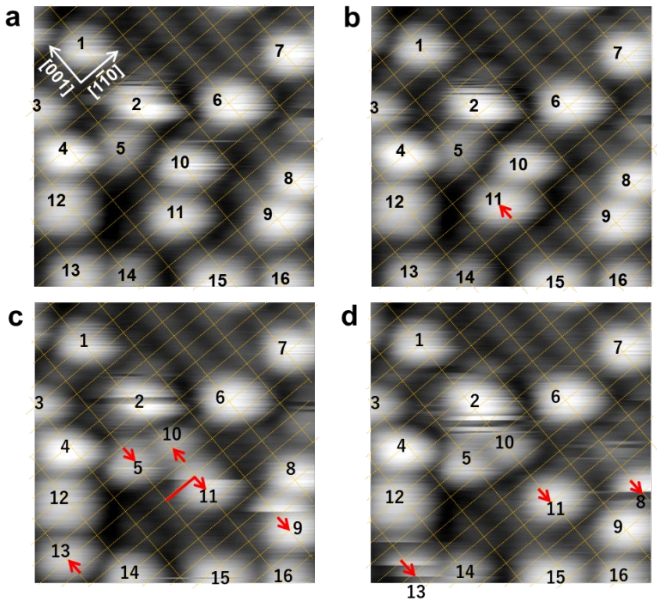

Figure 4. (a)-(d) Diffusion of methoxy intermediates on the Pt/TiO_2(110) surface at room temperature. The STM images were acquired 12 s per frame (5.0×5.0 nm^2). The Pt/TiO_2(110) surface was prepared by Pt deposition (0.01 ML) at room temperature, followed by annealing at 473 K for 10 min. The images were taken after exposure to 2 L methanol vapor at room temperature. The methoxy coverage was 0.09 ML. A 50×50 nm^2 scale image is shown in Figure S1.

No. 11 in the reverse direction by one lattice unit along the [001] direction. The adsorption of the two adjacent methoxy intermediates may be hindered by repulsive interaction between the intermediates. In the final frame shown in Figure 4d, methoxy No. 11 moved further away from No. 10 by one lattice unit along the [001] direction. In Figures 4c and 4d, the occasional migration of other methoxy species along the [001] direction was also observed, as indicated by the arrows. The methoxy species can thus move on the entire TiO_2(110) surface through diffusion along either the [001] or [1$\bar{1}$0] direction.

A series of DFT calculations was then conducted to obtain atomistic details into the diffusion processes of the methoxy intermediates. Firstly, we checked the adsorption energy of a methanol molecule on a TiO_2(110) surface when a single methanol molecule is adsorbed on a Ti_{5c} site with a p(4×2) unit cell, which corresponds to a methanol coverage of 0.125 ML and coincides well with the experimental results (0.14 ML). Figures S8a and S8b show the optimized structures of a methanol molecule adsorbed on a Ti_{5c} site in the forms of molecular and dissociated adsorption, respectively; the adsorption energies were calculated to be 1.19 eV and 1.38 eV, respectively. Dissociation is thus favored, which is consistent with the previous reports.[27,28] Once the methoxy species is formed on the TiO_2(110) surface by spillover from the Pt nanoparticles, it is energetically stabilized. The diffusion of the methoxy intermediate along the [001] direction was then examined. The direct hopping model shown in Figure S9 was initially tested. In this model, the methoxy species (CH_3O-Ti_{5c}) moves directly to the next Ti_{5c} site. The calculated diffusion barrier was 0.92 eV. The final state (Figure S9c) was less stable than the initial state (Figure S9a) by 0.13 eV, due to less interaction between the methoxy species and HO_{br}. The diffusion barrier can be decreased to 0.88 eV because the new methoxy species in Figure S9e was less stabilized and the transition state in Figure S9f was less affected by the HO_{br} species. Next, we tested a different model, the methanol-mediated model, as illustrated in Figure 5. In this model, the hydrogen atom of HO_{br} is transferred to the methoxy species to form a molecularly adsorbed methanol temporarily, which then migrates to the next Ti_{5c} site,

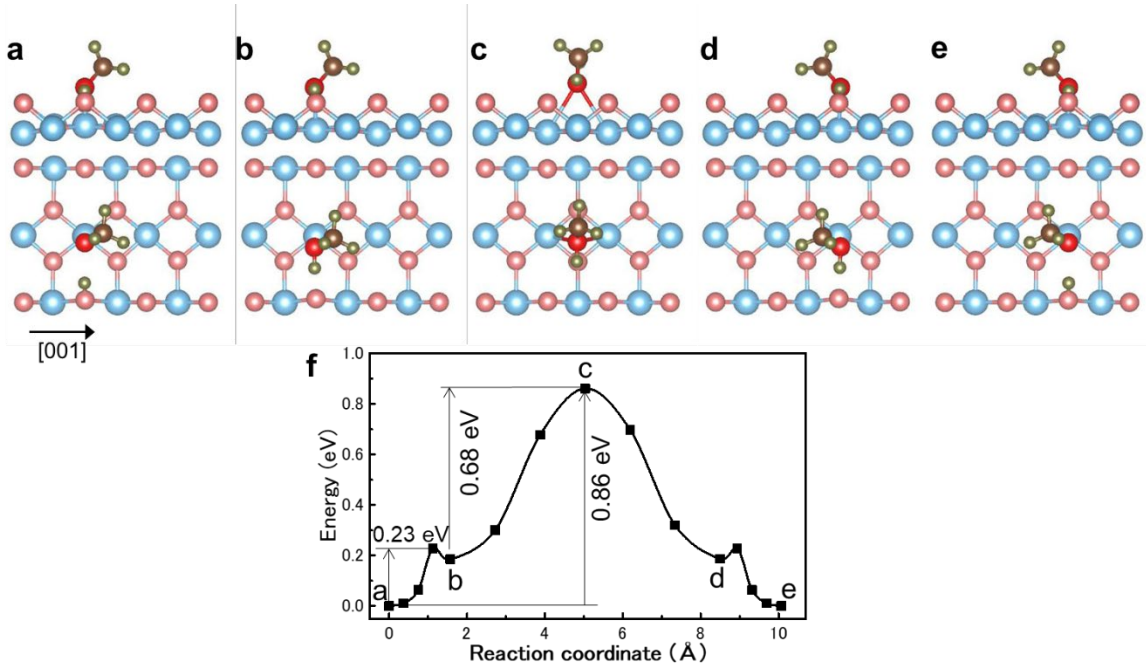

Figure 5. (a)-(e) Selected configurations in the (f) potential energy profile illustrating the diffusion of methoxy species along the [001] direction via molecularly adsorbed methanol (methanol-mediated model). Blue, red (pink), gray, and green balls represent Ti, O, C, and H atoms, respectively.

followed by the release of the hydroxyl hydrogen of the adsorbed methanol to the neighboring O_{br}. The energy difference between the states in Figures 5a and 5c was 0.86 eV, and the local minimum state was found at the state in Figure 5b, which is molecularly adsorbed methanol. The barrier to form the molecularly adsorbed methanol is rather small (0.23 eV) and it can diffuse to the next Ti_{5c} site with an activation energy as small as 0.68 eV, which was in agreement with the activation energy (0.65-0.85 eV) estimated in the previous STM study.[12] Considering the difference in the diffusion barriers between the two models, and the adsorption energy difference before and after hopping to the next Ti_{5c} site, the methanol-mediated model in Figure 5 is more likely than the direct hopping model in Figure S9. The methanol-mediated mechanism of methoxy diffusion on a solid surface is new to the best of the authors' knowledge.

The diffusion process along the [1$\bar{1}$0] direction was also examined. We first examined the diffusion path via a chain-like CH_3O-H-O_{br} intermediate, as shown in Figure S10 (1H model). After the CH_3O-Ti_{5c} bond is broken and the CH_3O-HO_{br} bond is subsequently formed, the CH_3O-H-O_{br} intermediate with the H-O_{br} hydrogen bond is formed at the transition state (see Figure S10b). The methoxy species is then reproduced on the Ti_{5c} site in the adjacent Ti row by breaking the CH_3O-HO_{br} bond and making the CH_3O-Ti_{5c} bond again. The barrier for this diffusion process was as high as 1.22 eV, which indicates that this process is less possible. The case where a methoxy species comes across two hydrogens (H_a and H_b) bonded to the two adjacent O_{br} atoms was then calculated, which is the 2H model shown in Figure 6. This situation can occur when the methoxy species of the methanol-mediated model in Figure 5 diffuses along the [001] direction and meets another hydroxyl group (HO_{br}). As shown in Figure S3, surface hydroxyl groups are originally present on the Pt/TiO_2(110) surfaces. In the 2H model, the hydrogen (H_a) of $H_aO_{a,br}$ is transferred to the methoxy species to form metastable molecularly adsorbed methanol, as shown in Figure 6b, and then the oxygen atom of the adsorbed methanol makes a bond with H_b of $H_bO_{b,br}$ after breaking the bond with Ti_{5c} (Figures 6b to 6d). In the conversion process of Figures 6b to 6d, the transition state was more stabilized compared with that of the 1H model in Figure S10 because the CH_3O species can interact with two hydrogens (H_a and H_b), and the metastable intermediate illustrated in Figure 6d can be formed. At the state shown in Figure 6d, the bond distances between the oxygen of CH_3O and the two hydrogens (H_a and H_b) are 0.99 Å and 1.68 Å, respectively, while those of H_a-$O_{a,br}$ and H_b-$O_{b,br}$ are 1.85 Å and 1.01 Å, respectively (see Figure S11). Therefore, CH_3O-H_b and H_a-$O_{a,br}$ form hydrogen bonds. This intermediate is then converted to the original state, which is CH_3O-Ti_{5c} + 2HO_{br} in Figure 6h via the states shown in Figures 6e to 6g. The highest activation energy of the elementary steps in this diffusion model was 0.64 eV. In the diffusion along the [1$\bar{1}$0] direction, interaction of the methoxy species with an additional hydrogen atom of the HO_{br} species was a key to stabilize the transition state and lower the diffusion barrier. A similar diffusion mechanism has been reported for the diffusion of ethanol molecules on a TiO_2(110) surface along the [1$\bar{1}$0] direction.[29] Enhanced molecular diffusion along the [001] direction assisted by HO_{br} has also been reported for catechol[30], water[31] and NO[32] molecules.

It is noted that the diffusion path in the 2H model took the adsorbed methanol state, which is similar to that in the methanol-mediated model shown in Figure 5; the activation energies were 0.64 eV and 0.68 eV, respectively, which

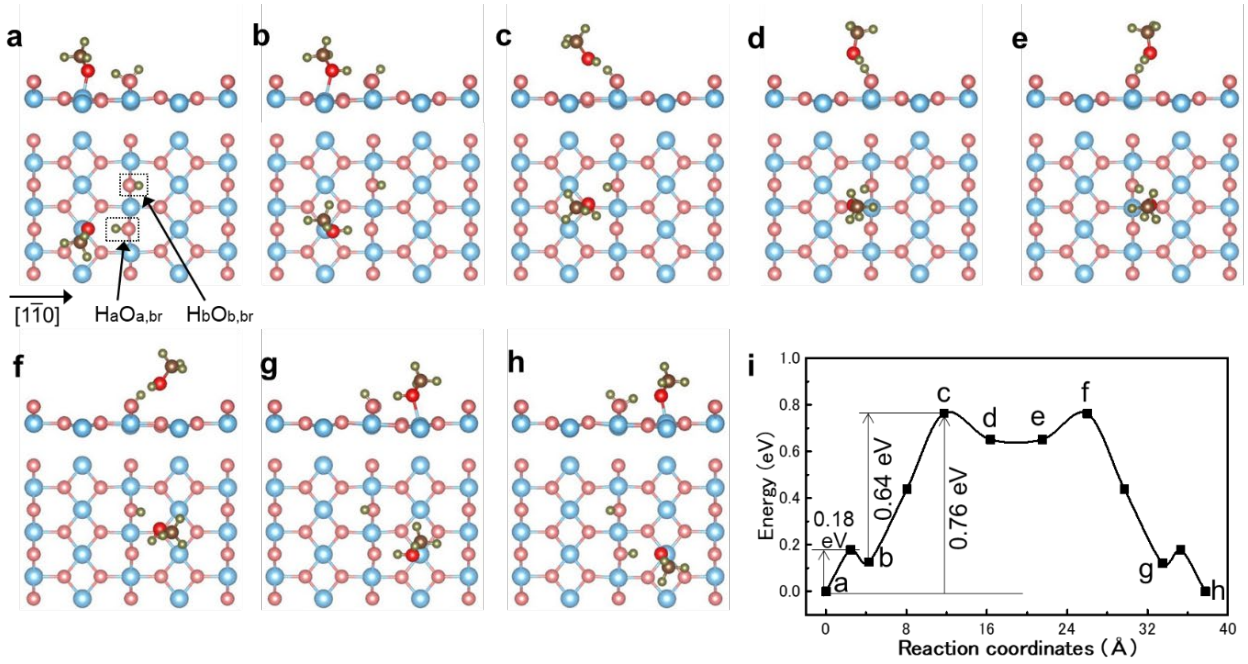

Figure 6. (a)-(h) Selected configurations in the (i) potential energy profile illustrating diffusion of methoxy species along the [1$\bar{1}$0] direction (2H model) in the presence of two adjacent hydrogen atoms (H_a and H_b bonded to $O_{a,br}$ and $O_{b,br}$, respectively). Blue, red (pink), gray, and green balls represent Ti, O, C, and H atoms, respectively.

are comparable. The difference between the two models is that the 2H model requires the interaction of the adsorbed methanol with an additional adjacent hydrogen (H_b of $H_bO_{b,br}$). In this sense, diffusion along the [1$\bar{1}$0] direction would be less frequent than that along the [001] direction. Preliminary estimation of rate constants for diffusion (diffusion coefficient, D [m²·s⁻¹]) along the [001] and [1$\bar{1}$0] directions was carried out as shown in Table S4. D can be expressed as $D = D_0\exp(-E/k_BT)$, where D_0, E, k_B, T are pre-exponential factor, activation energy, Boltzmann constant and temperature, respectively. The diffusion barriers calculated in Figures 5 and 6 (0.86 eV and 0.76 eV, respectively) were used as the activation energies. The D_0 values for diffusion along the [001] and [1$\bar{1}$0] directions were estimated to be 2×10^{-7} m²·s⁻¹ and 9×10^{-10} m²·s⁻¹, respectively. The latter value was more than two orders of magnitude lower than the former one, which would be because a methoxy intermediate (CH_3O-Ti+H-O_{br}) needs to find and meet an additional hydrogen of HO_{br}.

Our STM observations and DFT calculation results clearly show that the methoxy intermediates can diffuse over the entireTiO_2(110) surface, either along the [001] or [1$\bar{1}$0] direction, via the molecularly adsorbed methanol state with the aid of hydrogen adatoms bonded to O_{br}. Therefore, the methoxy intermediates can reach the active Pt sites where the decomposition reaction occurs, which is reflected in the TPD results shown in Figure 3, and can also be distributed homogeneously on the surface after spillover from the Pt nanoparticles in the methanol adsorption process.

Conclusion

We have studied the dynamic behavior of methoxy intermediates and its effect on methanol decompositionon the Pt/TiO_2(110) surface using STM, TPD, and DFT calculations. Methoxy intermediates were produced by the dissociative adsorption of methanol molecules on the Pt nanoparticles at room temperature, followed by spillover to the Ti_{5c} sites of the TiO_2(110) surface. The methoxy intermediates were distributed over the entire suface and thermally decomposed into CO and CH_4 at >350 K on the Pt sites through their reverse spillover. The activity for the decomposition reaction and the product selectivity were dependent on the Pt nanoparticle density, indicating that the diffusion of the methoxy intermedates can control the reaction. Sequential STM imaging showed that the methoxy intermediates diffuse along the [001] or [1$\bar{1}$0] direction, and can move over the entire surface. DFT calculations suggested that the formation of molecularly adsorbed methanol intermediates is a key for diffusion along the [001] and [1$\bar{1}$0] directions. They can move to the nearest neibor Ti_{5c} sites or to the Ti_{5c} sites located in the adjacent Ti_{5c} rows with activation energies less than 0.7 eV, which explains the facile approach of the methoxy intermediates to the Pt active sites where decomposition occurs. The present results clearly show how the intermediate adsorbates diffuse on the catalyst surface and reach the active sites to yield the corresponding products, and that atomic-level understanding of the dynamic behavior of intermediate adsorbates is crucial to elucidate the origins of catalytic activity and product selectivity in oxide-supported metal catalysts.

ASSOCIATED CONTENT

Supporting Information: additional experimental and calculation details; estimation of relative sensitivity factor and the selectivities of the products measured by TPD; estimation of rate constants for diffusion (diffusion coefficient, D[m²·s⁻¹]) of methoxy intermediates along the [001] and [1$\bar{1}$0] directions; dependence of methoxy coverage on methanol exposure for the H- and L-Pt/TiO_2(110) surfaces; STM image of the TiO2(110) surface after exposure to 5 L methanol at room temperature; densities of O_{br}, HO_{br} and pair of HO_{br} on the H- and L-Pt/TiO_2(110) surfaces; STM images of the H- and L-Pt/TiO_2(110) surfaces after heating at 650 K; Pt 4f XPS spectra of the H- and L-Pt/TiO_2(110) surfaces before and after heating at 650 K; TPD spectra from the bare TiO2(110) surface after exposure to methanol vapor at room temperature; wide scan STM image of Figure 4; DFT optimized structures of methanol adsorbed on TiO_2(110) surface; selected configurations and potential energy profiles of the methoxy direct hopping along [001] direction; selected configurations, energy profile, CH_3O-H and H-O_{br} distances of a methoxy species jumping over a H-O_{br} site along the [1$\bar{1}$0] direction; CH_3O-H_a, H_a-$O_{a,br}$, CH_3O-H_b and H_b-$O_{b,br}$ distances during the diffusion process of a methoxy species along the [1$\bar{1}$0] direction shown in Figure 6. This material is available free of charge via the Internet at http://pubs.acs.org.

AUTHOR INFORMATION

Corresponding Author

* E-mail: takakusa@cat.hokudai.ac.jp

Notes

The authors declare no competing financial interest.

ACKNOWLEDGMENT

This work was financially supported by the CREST projects (Nos. JPMJCR17J3 and JPMJCR19R3) of the Japan Science and Technology Agency (JST) and Kakenhi Grants-in-Aid (Nos. 18H01864, 18H05518, 21H01802 and 21H04650) from the Japan Society for the Promotion of Science (JSPS). The authors express their thanks to Mr. Haoran Xu (Hokkaido University) for his support in the XPS measurements. The authors also thank Mr. Yusuke Kawamura, Mr. Shingo Mukai, and Mr. Katsuhisa Ishikawa (Hokkaido University) for the design and preparation of the sample holder for the TPD measurements.

ABBREVIATIONS

STM, scanning tunneling microscopy; DFT, density functional theory; TPD, temperature-programmed desorption.

REFERENCES

(1) Dumesic, J. A.; Huber, G. W.; Boudart, M. *Handbook of heterogeneous catalysis*, 2nd ed.; Ertl, G., Knözinger, H., Schüth, F., Weitkamp, J., Eds.; Wiley-VCH: Weinheim, **2008**, Vol.1, 1-15.

(2) Somorjai, G. A.; Li, Y. *Introduction to Surface Chemistry and Catalysis*; 2 ed.; Wiley: Hoboken, NJ, **2010**, 1-38.

(3) Xiong, M.; Gao, Z.; Qin, Y. Spillover in Heterogeneous Catalysis: New Insights and Opportunities. *ACS Catal.* **2021**, *11*, 3159–3172.

(4) Delmon, B.; Froment, G. F. Remote Control of Catalytic Sites by Spillover Species: A Chemical Reaction Engineering Approach. *Catal. Rev.* **1996**, *38*, 69–100.

(5) Conner, W. C.; Falconer, J. L. Spillover in Heterogeneous Catalysis. *Chem. Rev.* **1995**, *95*, 759–788.

(6) Chen, B. S.; Falconer, J. L. Alcohol Decomposition by Reverse Spillover. *J. Catal.* **1993**, *144*, 214–1226.

(7) Green, R.; Morrall, P.; Bowker, M. CO Spillover and Oxidation on Pt/TiO2. *Catal. Lett.* **2004**, *98*, 129–1133.

(8) Onishi, H.; Fukui, K.-i.; Iwasawa, Y. Molecularly resolved observation of anisotropic intermolecular force in a formate-ion monolayer on a TiO2 (110) surface by scanning tunneling microscopy. C*olloids Surf. A Physicochem. Eng. Asp.* **1996**, 109, 335–343.

(9) Pedersen, M. Ø.; Österlund, L.; Mortensen, J. J.; Mavrikakis, M.; Hansen, L. B.; Stensgaard, I.; Lægsgaard, E.; Nørskov, J. K.; Besenbacher, F. Diffusion of N Adatoms on the Fe(100) Surface. *Phys. Rev. Lett.* **2000**, *84*, 4898.

(10) Xia, Y.; Zhang, B.; Ye, J.; Ge, Q.; Zhang, Z. Acetone-Assisted Oxygen Vacancy Diffusion on TiO2(110). *J. Phys. Chem. Lett.* **2012**, *3*, 2970–2974.

(11) Adamsen, K. C.; Kolsbjerg, E. L.; Koust, S.; Lammich, L.; Hammer, B.; Wendt, S.; Lauritsen, J. V. NH_3 on Anatase TiO2(101): Diffusion mechanisms and the Effect of Intermolecular Repulsion. *Phys. Rev. Mater.* **2020**, *4*, 121601(R).

(12) Takakusagi, S.; Fukui, K.-i.; Tero, R.; Asakura, K.; Iwasawa, Y. First Direct Visualization of Spillover Species Emitted from Pt Nanoparticles. *Langmuir* **2010**, *26*, 16392–16396.

(13) Zhang, Z.; Bondarchuk, O.; White, J.M.; Kay, B.D.; Dohnálek, Z. Imaging Adsorbate O–H Bond Cleavage: Methanol on TiO_2(110)., *J. Am. Chem. Soc.* **2006**, *128*, 4198–4199.

(14) Zheng, Q.; Tan, S.; Feng, H.; Cui, X.; Zhao, J.; Wang, B. Dynamic Equilibrium of Reversible Reactions and Migration of Hydrogen Atoms Mediated by Diffusive Methanol on Rutile TiO_2(110)-(1 × 1) Surface. *J. Phys.Chem. C* **2016**, *120*, 7728–7735.

(15) Tenney, S. A.; Shah, S. I.; Yan, H.; Cagg, B. A.; Levine, M. S.; Rahman, T. S.; Chen, D. A. Methanol Reaction on Pt–Au Clusters on TiO2(110): Methoxy-Induced Diffusion of Pt. *J. Phys. Chem. C* **2013**, *117*, 26998–27006.

(16) Sexton, B.A. Methanol decomposition on platinum (111). *Surf. Sci.* **1981**, *102*, 271-281.

(17) Gibson, K.D.; Dubois, L.H. Step effects in the thermal decomposition of methanol on Pt(111). *Surf. Sci.* **1990**, *233*, 59-64.

(18) Kizhakevariam, N.; Stuve, E.M. Promotion and poisoning of the reaction of methanol on clean and modified platinum (100). *Surf. Sci.* **1993**, *286*, 246-260.

(19) Chao, C.-S.; Li, Y.-D.; Hsu, B.-W.; Lin, W.-R.; Hsu, H.-C.; Hung, T.-C.; Wang, C.-C.; Luo, M.-F. Two-Channel Decomposition of Methanol on Pt Nanoclusters Supported on a Thin Film of Al_2O_3/NiAl(100). *J. Phys. Chem. C* **2013**, *117*, 5667–5677.

(20) Hao, Q.; Wang, Z.; Wang, T.; Ren, Z.; Zhou, C.; Yang, X. Role of Pt Loading in the Photocatalytic Chemistry of Methanol on Rutile TiO_2(110). *ACS Catal.* **2019**, *9*, 286–294.

(21) Hugenschmidt, M.B.; Gamble, L.; Campbell, C.T. The interaction of H_2O with a TiO_2(110) surface. *Surf. Sci.* **1994**, *302*, 329–340.

(22) Henderson, M.A.; Epling, W.S.; Peden, C.H.F.; Perkins, C.L. Insights into Photoexcited Electron Scavenging Processes on TiO_2 Obtained from Studies of the Reaction of O_2 with OH Groups Adsorbed at Electronic Defects on TiO_2(110). *J. Phys. Chem. B* **2003**, *107*, 534–545.

(23) Ammal, S.C.; Heyden, A. Modeling the noble metal/TiO_2 (110) interface with hybrid DFT functionals: A periodic electrostatic embedded cluster model study. *J. Chem. Phys.* **2010**, *133*, 164703.

(24) Fu, J.; Lym, J.; Zheng, W.; Alexopoulos, K.; Mironenko, A. V.; Li, N.; Boscoboinik, J. A.; Su, D.; Weber, R. T.; Vlachos, D. G. C–O bond Activation Using Ultralow Loading of Noble Metal Catalysts on Moderately Reducible Oxides. *Nat. Catal.* **2020**, *3*, 446–453.

(25) Phillips, K. R.; Jensen, S. C.; Baron, M.; Li, S.-C.; Friend, C. M. Sequential Photo-oxidation of Methanol to Methyl Formate on TiO2(110). *J. Am. Chem. Soc.* **2013**, *135*, 574–577.

(26) Henderson, M. A.; Otero-Tapia, S.; Castro, M. E. The Chemistry of Methanol on the TiO2(110) Surface: the Influence of Vacancies and Coadsorbed Species. *Faraday Discuss.* **1999**, *114*, 313–329.

(27) Silber, D.; Kowalski, P. M.; Traeger, F.; Buchholz, M.; Bebensee, F.; Meyer, B.; Wöll, C. Adsorbate-induced Lifting of Substrate Relaxation Is a General Mechanism Governing Titania Surface Chemistry. *Nat. Commun.* **2016**, *7*, 12888.

(28) Sun, K.; Su, H.-Y.; Li, W.-X. Structures and Stability of Adsorbed Methanol on TiO2(110) Surface Studied by ab initio Thermodynamics and Kinetic Monte Carlo Simulation. *Theor. Chem. Acc.* **2018**, *137*, 128.

(29) Huo, P.; Hansen, J. Ø.; Martinez, U.; Lira, E.; Streber, R.; Wei, Y.; Lægsgaard, E.; Hammer, B.; Wendt, S.; Besenbacher, F. Ethanol Diffusion on Rutile TiO2(110) Mediated by H Adatoms. *J. Phys. Chem. Lett.* **2012**, *3*, 283–288.

(30) Li, S.-C.; Chu, L.-N.; Gong, X.-Q.; Diebold, U. Hydrogen Bonding Controls the Dynamics of Catechol Adsorbed on a TiO_2(110) Surface. *Science* **2010**, *328*, 882–884.

(31) Matthiesen, J.; Hansen, J.Ø;. Wendt, S.; Lira, E.; Schaub, R.; Lægsgaard, E.; Besenbacher, F.; Hammer, B. Formation and Diffusion of Water Dimers on Rutile TiO_2(110). *Phys. Rev. Lett.* **2009**, *102*, 226101.

(32) Yu, Y.-Y.; Diebold, U.; Gong, X.-Q. NO adsorption and diffusion on hydroxylated rutile TiO_2(110). *Phys. Chem. Chem. Phys.* **2015**, *17*, 26594--26598.

For Table of Contents Only

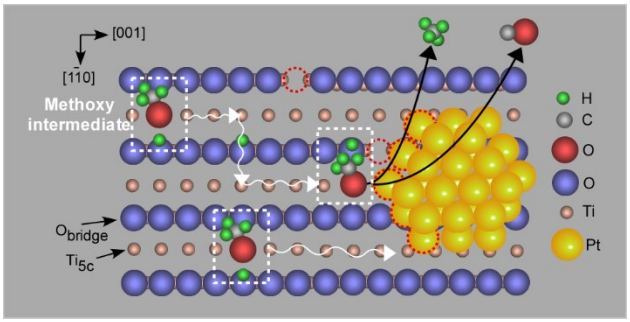

Supporting Information
Dynamic Behavior of Intermediate Adsorbates to Control Activity and Product Selectivity in Heterogeneous Catalysis: Methanol Decomposition on Pt/TiO_2(110)

Can Liu,[a] Bang Lu,[b] Hiroko Ariga-Miwa,[c] Shohei Ogura,[d] Takahiro Ozawa,[e] Katsuyuki Fukutani,[e] Min Gao,[f] Jun-ya Hasegawa,[a] Ken-ichi Shimizu,[a] Kiyotaka Asakura,[a] and Satoru Takakusagi*[a]

[a] Institute for Catalysis, Hokkaido University, Sapporo, Hokkaido 001-0021, Japan

[b] Division of Quantum Science and Engineering, Graduate School of Engineering, Hokkaido University, Sapporo, Hokkaido 001-0021, Japan

[c] Innovation Research Center for Fuel Cells, The University of Electro-Communications, 1-5-1 Chofugaoka, Chofu, Tokyo 182-8585, Japan

[d] School of Engineering, Tokyo Denki University, 5 Senju Asahi-cho, Adachi-ku, Tokyo 120-8 551, Japan

[e] Institute of Industrial Science, The University of Tokyo, 4-6-1 Komaba, Meguro-ku, Tokyo 153-8505, Japan

[f] Institute for Chemical Reaction Design and Discovery (ICReDD), Hokkaido University, Sapporo, Hokkaido 001-0021, Japan

* Corresponding Author:

Satoru Takakusagi. E-mail: takakusa@cat.hokudai.ac.jp

Experimental procedures

All experiments were performed in an ultra-high vacuum (UHV) chamber with a base pressure below 3×10^{-8} Pa. As-received rutile-TiO_2(110) wafer (Shinkosha Co., Japan) was first immersed in 10% HF solution, and then calcined in air at 1100 K for 12 h.[1,2] After being loaded into the UHV chamber, the wafer was cleaned by cycles of Ar^+ sputtering (2 keV) and vacuum annealing (1000 K) to obtain an atomically flat TiO_2(110)-(1×1) surface. Pt was deposited at room temperature by Pt vapor generation through electron bombardment of a Pt rod (99.98%, Nilaco Co., Japan) with application of a high voltage (typically 850 V) between the filament and the Pt rod. The Pt coverage was estimated from the X-ray photoelectron spectroscopy (XPS) peak area ratio of Pt $4f_{7/2}$−Ti $2p_{3/2}$, where 1 ML was defined as the density of the (1×1) units of the TiO_2(110) surface, i.e., 5.2×10^{18} /m^2. After Pt deposition at room temperature, the Pt/TiO_2(110) surface was annealed at 473 K for 10 min in the UHV chamber to obtain a uniform size distribution of Pt nanoparticles. Methanol (Superpure reagent grade, Fujifilm Wako Chemicals, Japan) was purified by several freeze-pump-thaw cycles using liquid nitrogen prior to introduction onto the Pt/TiO_2(110) surface and was dosed at room temperature through a variable leak valve by backfilling.

STM measurements were conducted using a JEOL JSPM4500S microscope. Images were recorded using an electrochemically etched W tip at room temperature, with a sample bias voltage of +1.2–2.6 V and a tunneling current of 0.1–0.2 nA. Temperature-programmed desorption (TPD) measurements were performed by heating the sample surface from room temperature to 700 K at ca. 2 K/s using shielded and differentially pumped quadrupole mass spectrometer.[3] All TPD spectra were normalized with respect to the heating rate.

Density functional theory (DFT) calculations were performed using VASP 5.4[4-7] with the projector augmented wave (PAW) and plane-wave basis set methods.[8] The kinetic energy cutoff for plane-wave expansion was set to 400 eV, and the exchange-correlation interaction between electrons was described by the Perdew-Burke-Ernzerhof functional (PBE).[9,10] TiO_2(110) surfaces were modeled as a five TiO_2 trilayer slab with a (4×2) unit cell. The vacuum layer was 20 Å. The bottom two layers were fixed throughout calculations, while the upper three trilayers and the adsorbates were relaxed using a quasi-Newton algorithm until the energy difference was smaller than 10^{-5} eV. The k-point mesh was set as 2×2×1. The climbing nudged elastic band (NEB)[11] method was used to calculate the diffusion and dissociation barriers.

Table S1. Estimation of relative sensitivity factor (RSF) for carbon monoxide, methane, formaldehyde, and methanol in the quadrupole mass spectrometer used in the TPD measurements. RSF can be expressed as $RSF=R_S \times R_F \times R_Q$, where R_S, R_F, and R_Q are the source sensitivity factor,[a] the fragmentation factor,[b] and the quadrupole transmission,[c] respectively. The RSF values were normalized assuming the RSF value for a nitrogen molecule (N_2) to be 1.00.

	Base peak	R_S	R_F	R_Q	RSF
Carbon monoxide (CO)	28.00	1.00	0.93	1.00	1.07
Methane (CH_4)	16.00	1.41	0.44	1.00	0.72
Formaldehyde (H_2CO)	30.00	1.64	0.31	1.00	0.58
Methanol (CH_3OH)	31.00	1.77	0.41	1.00	0.83
Nitrogen molecule (N_2)	28.00	1.00	0.87	1.00	1.00

[a] Cited from the NIST database on electron-impact ionization cross sections for 70 eV[12] and Ref. [13].
[b] Cited from the NIST database.[14]
[c] The quadrupole transmission can be regarded as effectively constant in the mid-mass region (16–40).[15] Therefore, the R_Q value was assumed to be 1.00 for all the gases.

Table S2. Estimation of the selectivity toward carbonaceous products (CO, CH_4, H_2CO, and CH_3OH) from TPD spectra for the H-Pt/TiO_2(110) sample.

	CO	CH_4	H_2CO	CH_3OH
(1) TPD peak area	3.34×10^{-9}	3.78×10^{-9}	5.21×10^{-10}	3.70×10^{-10}
(2) (1) divided by RSF [a]	3.12×10^{-9}	5.26×10^{-9}	8.98×10^{-10}	4.46×10^{-10}
(3) Product amount [b]	2.96×10^{-9}	5.25×10^{-9}	8.98×10^{-10}	4.46×10^{-10}
(4) Product selectivity (%) [c]	31	55	9	5

[a] The RSF value for each product was taken from Table S1.
[b] The amount of CO product was calculated by subtracting the fragmentation from H_2CO and CH_3OH, and the amount of CH_4 by subtracting the fragmentation from CH_3OH. The total product amount was 9.6×10^{-9}.
[c] Product selectivity was defined as the ratio (%) of the target product amount to the total product amount.

Table S3. Estimation of the selectivity toward carbonaceous products (CO, CH_4, H_2CO, and CH_3OH) from TPD spectra for the L-Pt/TiO_2(110) sample.

	CO	CH_4	H_2CO	CH_3OH
(1) TPD peak area	1.15×10^{-9}	4.72×10^{-9}	3.84×10^{-10}	2.25×10^{-10}
(2) (1) divided by RSF [a]	1.08×10^{-9}	6.55×10^{-9}	6.62×10^{-10}	2.71×10^{-10}
(3) Product amount [b]	9.89×10^{-10}	6.55×10^{-9}	6.62×10^{-10}	2.71×10^{-10}
(4) Product selectivity (%) [c]	12	77	8	3

[a] The RSF value for each product was taken from Table S1.
[b] The amount of CO product was calculated by subtracting the fragmentation from H_2CO and CH_3OH, and the amount of CH_4 by subtracting the fragmentation from CH_3OH. The total product amount t was 8.5×10^{-9}.
[c] Product selectivity was defined as the ratio (%) of the target product amount to the total product amount.

Table S4. Estimation of rate constants for hopping (ν [s^{-1}]) and diffusion (D [$m^2 \cdot s^{-1}$]) of methoxy intermediates on $Pt/TiO_2(110)$ along $[001]$ and $[1\bar{1}0]$ directions. [a]

	ν_0 [s^{-1}] [b]	D_0 [$m^2 \cdot s^{-1}$] [c]	E [eV]
Hopping ν, $[001]$ direction	4×10^{12}	-	0.86
Diffusion D, $[001]$ direction	-	2×10^{-7}	0.86
Hopping ν, $[1\bar{1}0]$ direction	9×10^{9}	-	0.76
Diffusion D, $[1\bar{1}0]$ direction	-	9×10^{-10}	0.76

[a] ν and D can be expressed as $\nu = \nu_0 \exp(-E/k_BT)$ and $D = D_0 \exp(-E/k_BT)$, respectively. ν_0 and D_0 are pre-exponential factors for the hopping and diffusion prcesses, respectivly, and E, k_B, T are activation energy, Boltzmann constant and temperature, respectively. The diffusion barriers calculated in Figures 5 and 6 (0.86 eV and 0.76 eV along the $[001]$ and $[1\bar{1}0]$ directions, respectively) were used as the activation energies.

[b] Firstly, ν at T=300 K was estimated from the sequential STM images in Figure 4. For example, since 9 methoxy intermediates among the total 16 ones moved along the $[001]$ direction in Figures 4a to 4d (36 s), ν was determined to be 0.016 s^{-1}. And then ν_0 was calculated using $\nu = \nu_0 \exp(-E/k_BT)$, where ν, E, k_BT are 0.016 s^{-1}, 0.86 eV and 0.026 eV, respectively. ν_0 for diffusion along the $[1\bar{1}0]$ direction was estimated in the similar manner.

[c] D_0 was calculated using the equation $D = l^2/(4\tau)$, where l and τ are jump length and average lifetime of a adsorbate at the stable binding sites, respectively.[16, 17] In the case of diffusion along the $[001]$ direction, the jump length is the distance between the nearest neibor Ti_{5c} sites (0.30 nm), while from each Ti_{5c} site the methoxy species can hop to two neighboring Ti_{5c} sites. Therefore the average lifetime at the Ti_{5c} sites is given by $\tau = 1/(2\nu)$. Similarly, l and τ for diffusion along the $[1\bar{1}0]$ direction were determined be 0.65 nm and $1/\nu$, respectivly.

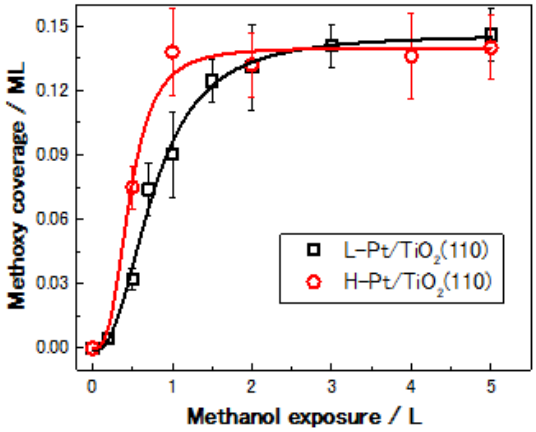

Figure S1. Dependence of methoxy coverage on methanol exposure for the $Pt/TiO_2(110)$ surfaces loaded with 0.04 ML Pt (L-$Pt/TiO_2(110)$, black open squares) and 0.11 ML Pt (H-$Pt/TiO_2(110)$, red open circles), respectively. The surfaces were annealed at 473 K for 10 min after Pt deposition at room temperature and then subjected to methanol exposure at room temperature.

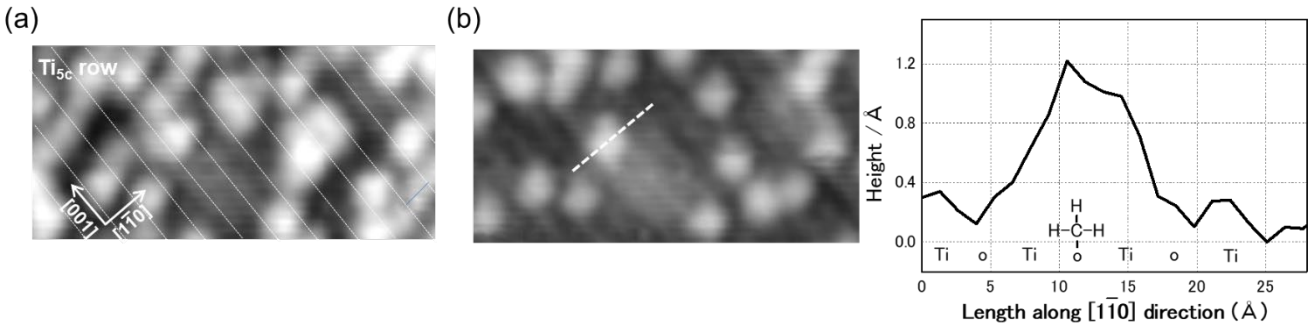

Figure S2. (a) STM image of the $TiO_2(110)$ surface after exposure to 5 L methanol at room temperature. Scale: 4×8 nm^2. (b) STM image of the same area after removal of the hydroxyl groups by applying the high bias sweep (3.0 V), and the line profile across the white dotted line in the STM image. The bright spots are located on the bridging oxygen (O_{br}) rows and are suggested to be the methoxy species filling the O_{br} vacancies.

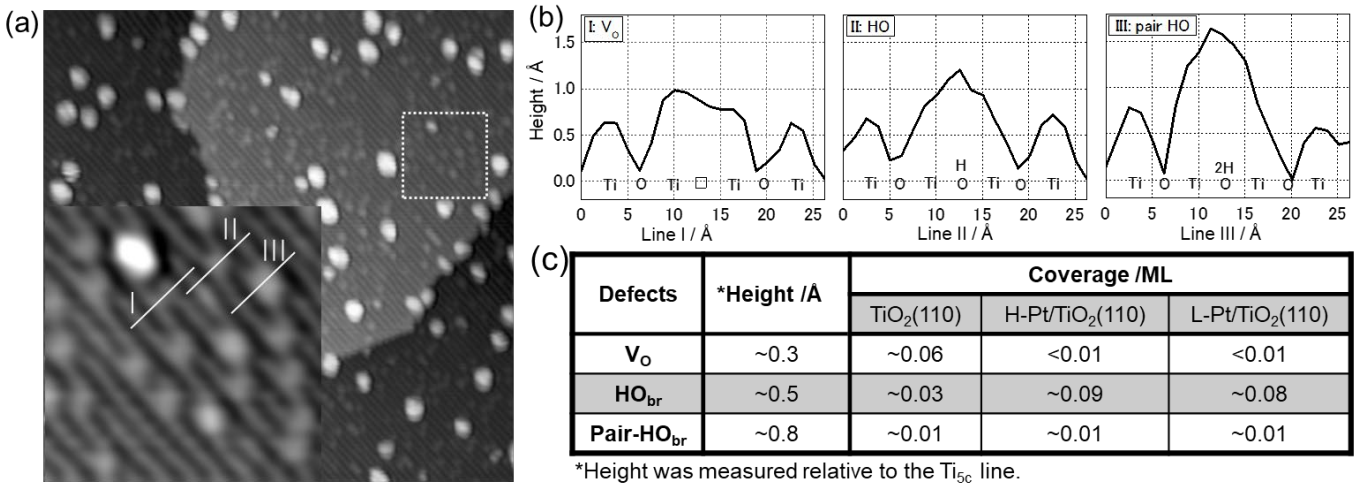

(c)

Defects	*Height /Å	Coverage /ML		
		TiO_2(110)	H-Pt/TiO_2(110)	L-Pt/TiO_2(110)
V_O	~0.3	~0.06	<0.01	<0.01
HO_{br}	~0.5	~0.03	~0.09	~0.08
Pair-HO_{br}	~0.8	~0.01	~0.01	~0.01

*Height was measured relative to the Ti_{5c} line.

Figure S3. (a) STM image (50×50 nm^2) of the L-Pt/TiO_2(110) surface (same image as Figure 2a in the manuscript). The inset shows the magnified image marked by the white dotted square. (b) The line profiles across three different kinds of bright spots in the inset of (a). According to their shapes and heights, they are assigned to oxygen vacancies (V_O), hydroxyls (HO_{br}), and pair of hydroxyls (pair-HO_{br}), respectively. (c) The apparent heights and coverages of the three species on the clean TiO_2(110) surface, L-Pt/TiO_2(110), and H-Pt/TiO_2(110) surfaces.

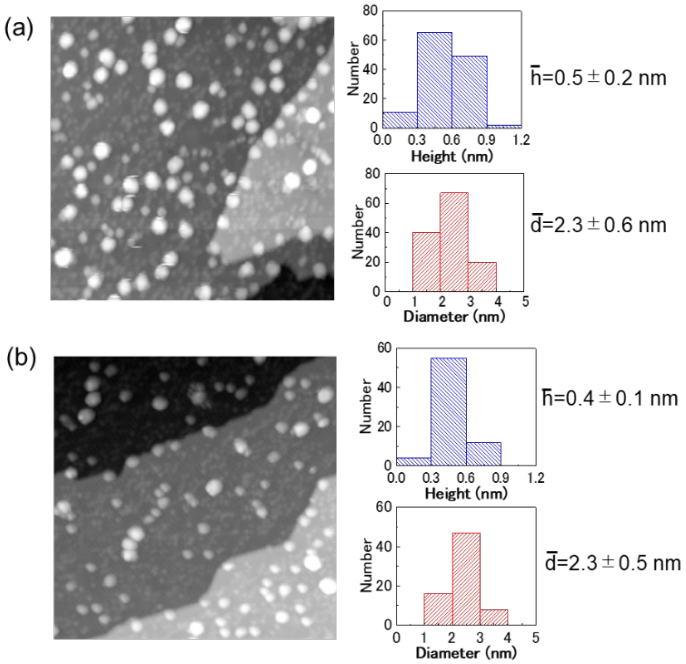

Figure S4. STM images and the histograms of the Pt nanoparticles of the H- and L-Pt/TiO_2(110) surfaces after heating at 650 K for 1 min. (a) H-Pt/TiO_2(110) surface with 0.11 ML Pt. (b) L-Pt/TiO_2(110) surface with 0.04 ML Pt. The images were measured at room temeperature. Scale: 50×50 nm^2.

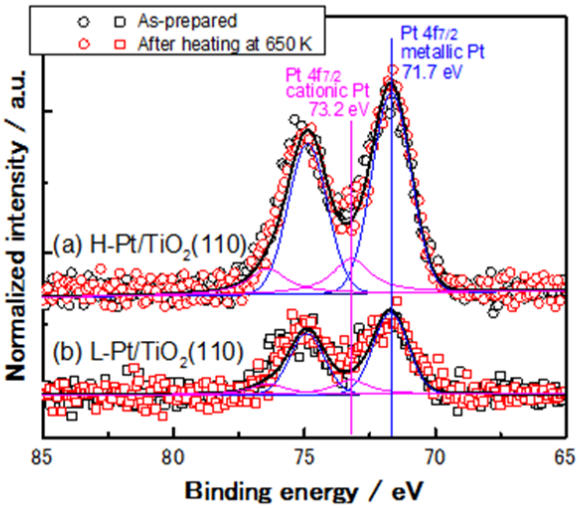

Figure S5. Pt 4f XPS spectra of the H- and L-Pt/TiO_2(110) surfaces before and after heating at 650 K. (a) H-Pt/TiO_2(110) (0.11 ML Pt). (b) L-Pt/TiO_2(110) (0.04 ML Pt). The black open circles and squares represent the as-prepared H- and L-Pt/TiO_2(110) surfaces, respectively, which were annealed at 473 K for 10 min after Pt deposition at room temperature. The red open circles and squares represent the H- and L-Pt/TiO_2(110) surfaces, respectively, afte additional heating at 650 K for 1 min. The solid black lines are the fitted curves of the Pt 4f spectra for the H- and L-Pt/TiO_2(110) surfaces after the additional heating. The ratio of the Pt $4f_{5/2}$ to the Pt $4f_{7/2}$ peak area was fixed to be 0.75. The FWHM of the deconvoluted peaks was 1.7±0.1 eV. The Pt $4f_{7/2}$ peaks at 71.7 and 73.2 eV were tentatively assigned to metallic and cationic Pt atoms, respectively. The cationic Pt atoms could be formed at the Pt-TiO_2 interface. The ratio of the cationic Pt to the metallic Pt peak area was ~0.3 for both samples.

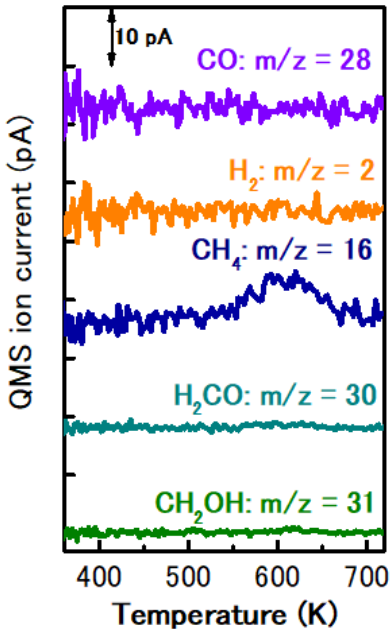

Figure S6. TPD spectra from the TiO_2(110) surface after exposure to 5 L methanol at room temperature.

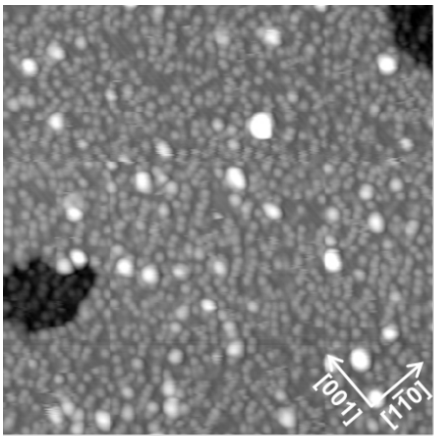

Figure S7. Wide scan STM image (50×50 nm^2) of the $Pt/TiO_2(110)$ surface shown in Figure 4, which was obtained after exposure to 2 L methanol vapor at room temperature. The methoxy coverage was 0.09 ML. The $Pt/TiO_2(110)$ surface was prepared by Pt deposition (0.01 ML) at room temperature, followed by annealing at 473 K for 10 min.

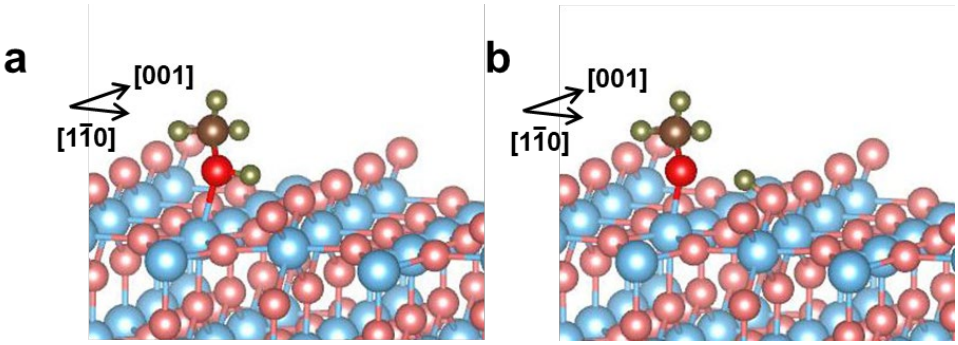

Figure S8. Optimized structures of methanol adsorbed on a Ti_{5c} site of the $TiO_2(110)$ surface. (a) Molecular adsorption. (b) Dissociative adsorption. Blue, red (pink), gray, and green balls represent Ti, O, C, and H atoms, respectively. Adsorption energies for (a) and (b) were 1.19 and 1.38 eV, respectively.

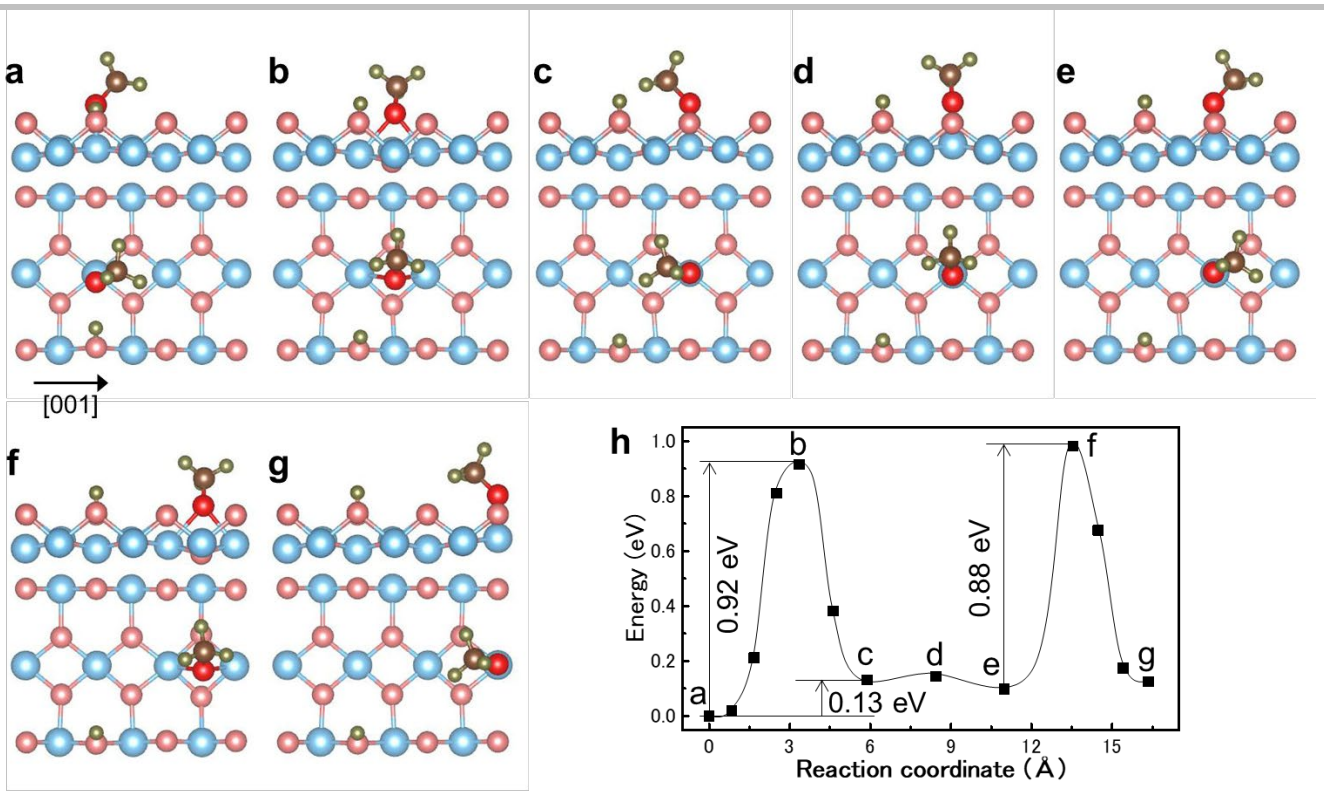

Figure S9. (a)-(g) Selected configurations in the (h) potential energy profile illustrating diffusion of a methoxy species along the [001] direction (direct hopping model). Blue, red (pink), gray, and green balls represent Ti, O, C, and H atoms, respectively.

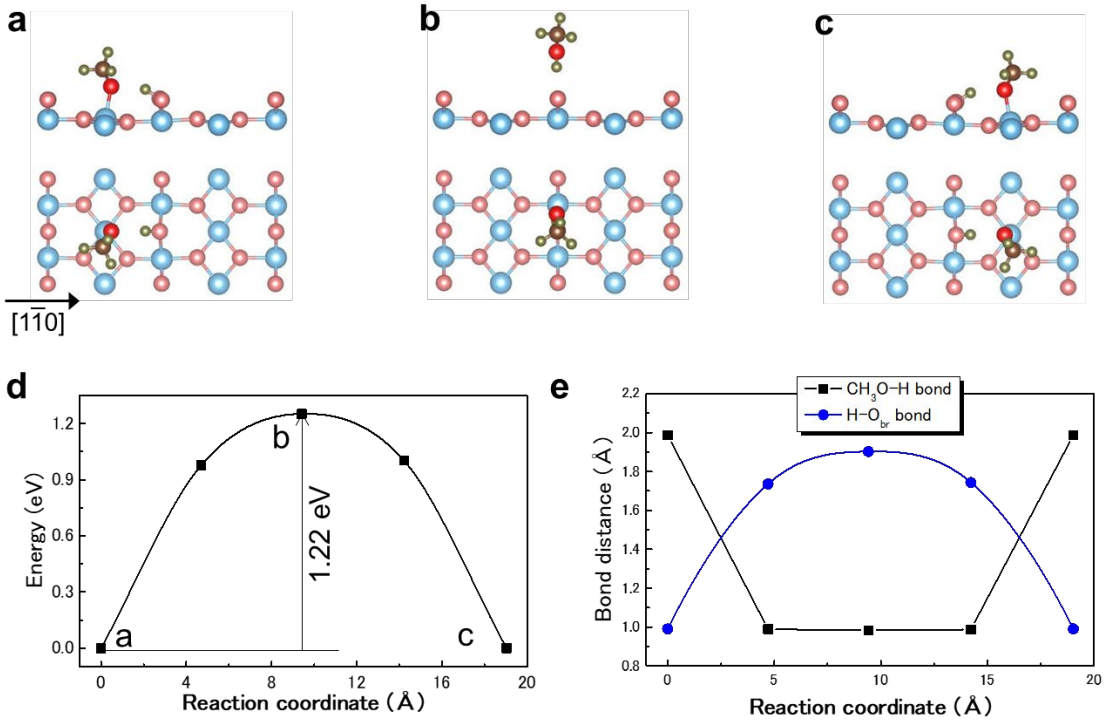

Figure S10. (a)-(c) Selected configurations in the (d) energy profile illustrating diffusion of a methoxy species over a H-O_{br} site along the [1$\bar{1}$0] direction. (e) CH_3O-H and H-O_{br} distances during the diffusion process. Blue, red (pink), gray, and green balls represent Ti, O, C, and H atoms, respectively.

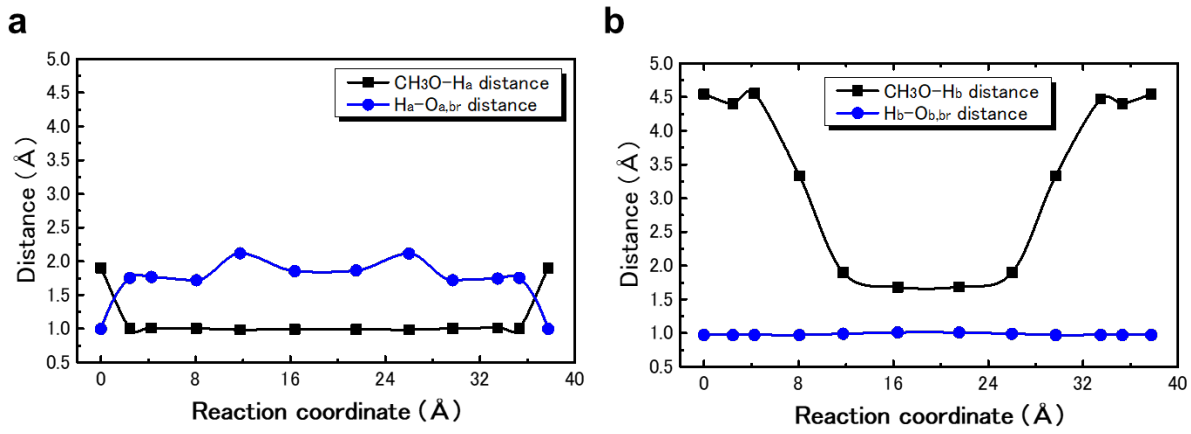

Figure S11. (a) CH_3O-H_a and H_a-$O_{a,br}$ distances and (b) CH_3O-H_b and H_b-$O_{b,br}$ distances during the diffusion process of the methoxy species along the [1$\bar{1}$0] direction shown in Figure 6. See Figure 6a for the locations of H_a, $O_{a,br}$, H_b, and $O_{b,br}$.

References

(1) Yamamoto, Y.; Nakajima, K.; Ohsawa, T.; Matsumoto, Y.; Konuma, H. *Jpn. J. Appl. Phys., Part 2* **2005**, *44*, L511.
(2) Nakamura, R.; Ohashi, N.; Imanishi, A.; Osawa, T.; Matsumoto, Y.; Koinuma, H.; Nakato, Y. *J. Phys. Chem. B* **2005**, *109*, 1648.
(3) Ogura, S.; Okada, M.; Fukutani, K. *J. Phys. Chem. C* **2015**, *119*, 23973.
(4) Kresse, G.; Hafner, J. *Phys. Rev. B* **1993**, *47*, 558.
(5) Kresse, G.; Hafner, J. *Phys. Rev. B* **1994**, *49*, 14251.
(6) Kresse, G.; Furthmüller, J. *Comput. Mat. Sci.* **1996**, *6*, 15.
(7) Kresse, G.; Furthmüller, J. *Phys. Rev. B* **1996**, *54*, 11169.
(8) Blöchl, P. E. *Phys. Rev. B* **1994**, *50*, 17953.
(9) Perdew, J. P.; Burke, K.; Ernzerhof, M. *Phys. Rev. Lett.* **1996**, *77*, 3865.
(10) Perdew, J. P.; Burke, K.; Ernzerhof, M. *Phys. Rev. Lett.* **1997**, *78*, 1396.
(11) Henkelman, G.; Jónsson, H. *J. Chem. Phys.* **2000**, *113*, 9978.
(12) https://physics.nist.gov/PhysRefData/Ionization/intro.html.
(13) Srivastava, S. K.; Krishnakumar, E.; Fucaloro, A. F.; van Note, T. *J. Geophys. Res.* **1996**, *101*, 26155.
(14) https://webbook.nist.gov/chemistry/.
(15) In Application Note 282; Hiden Analytical, Ltd.
(16) Borodin, D.; Galparsoro, O.; Rahinov, I.; Fingerhut, J.; Schwarzer, M.; Hörandl, S.; Auerbach, D. J.; Kandratsenka, A.; Schwarzer, D.; Kitsopoulos, T. N.; Wodtke, A. M.. *J. Am. Chem. Soc.*, **2022**, *144*, 21791.
(17) King, D. A. *J. Vac. Sci. Technol.*, **1980**, *17*, 241.